Available online at www.sciencedirect.com
SCIENCE DIRECT®
Scripta Materialia 52 (2005) 335–339
Scripta MATERIALIA
www.actamat-journals.com

Processing and structure of open-celled amorphous metal foams

A.H. Brothers, R. Scheunemann, J.D. DeFouw, D.C. Dunand *

Department of Materials Science and Engineering, Northwestern University, 2220 Campus Drive, Evanston, IL 60208, USA

Received 27 September 2004; accepted 1 October 2004
Available online 2 November 2004

Abstract

Amorphous metallic foams with an open-cell structure are processed with the salt replication method by infiltration of a sintered salt pattern with liquid Vit106, a Zr-based bulk metallic glass. After pattern removal in nitric acid, the Vit106 foams exhibit highly uniform pores, about 250 μm in size, and relative densities in the range 15–22%. Processing parameters, including pattern selection, sintering, and removal, are investigated.

Keywords: Metallic glasses; Foams; Foaming; Liquid infiltration; Processing

1. Introduction

Metallic foams exhibit a unique combination of properties, including high density-compensated mechanical properties (e.g., strength, stiffness, damping and energy absorption capacity) [1,2]. Until very recently, all metallic foams were made from conventional crystalline alloys, mostly Al-based [1]. It was not until the development of bulk metallic glasses (BMG) with high glass-forming ability [3,4] that methods for processing of amorphous metal foams became feasible. Apfel and Qiu [5] were the first to suggest a method for processing of BMG foams based on gas expansion, but never demonstrated its use with a BMG alloy. Recently, Schroers et al. [6] demonstrated the first BMG foam by entrapping gas in a liquid $Pd_{43}Ni_{10}Cu_{27}P_{20}$ alloy (all compositions are given in at.% hereafter). Wada and Inoue [7] reported foaming of the same alloy by casting around soluble NaCl placeholders. Shortly thereafter, Brothers and Dunand [8] developed an alternative method based on liquid infiltration of carbon cenospheres, appropriate for use with reactive commercial BMG alloys, e.g. Zr-based alloys. While strong evidence demonstrating plasticity in BMG foams is still lacking, Conner et al. [9] have compiled extensive literature documenting high bending ductility in sub-millimeter amorphous metal wires and foils. The similarity between amorphous metal wires and the struts of an amorphous metal foam with open-celled architecture, combined with the fact that the struts of a low-connectivity, open-celled foam deform in bending even during uniaxial compression of the foam, motivates the hypothesis that open-celled BMG foams with low connectivity can show high ductility in compression, making them useful in various structural applications [1].

In this report, a novel method for processing of open-celled foams from the commercial BMG alloy Vit106 ($Zr_{57}Nb_5Cu_{15.4}Ni_{12.6}Al_{10}$) is described, and parameters controlling the foaming process are explored and discussed. This method is based on the salt replication process used as early as 1961 in the production of aluminum foams [10], and more recently carbon [11], SiC [12], and amorphous Pd-based [7] foams, but differs

* Corresponding author. Tel.: +1 847 491 5370/467 3996; fax: +1 847 491 7820.
E-mail address: dunand@northwestern.edu (D.C. Dunand).

1359-6462/$ - see front matter © 2004 Acta Materialia Inc. Published by Elsevier Ltd. All rights reserved.
doi:10.1016/j.scriptamat.2004.10.002

from earlier work in the use of refractory fluoride salts in place of NaCl. To the authors' knowledge, this report represents the first such extension of the method to a salt different from NaCl. Though the modified method makes strict demands on the corrosion resistance of the alloy to be foamed, it is thought to be otherwise applicable to the production of low-density foams from other amorphous or crystalline high-melting alloys.

2. Experimental procedures

SrF_2 powders (180–355 μm) and BaF2 powders (212–250 μm) were prepared by crushing monocrystalline pieces of optical-grade (99.999+%) SrF_2 and BaF_2. Sieved powders were packed in graphite crucibles and sintered for 10 h at temperatures of 1400–1440 °C (for SrF_2) and 1200–1350 °C (for BaF_2) in three different atmospheres: high vacuum, low vacuum, and argon cover gas. Sintered patterns for infiltration were placed in thin-walled (0.75 mm) stainless steel crucibles and vacuum-dried at 300 °C for at least 30 min. After drying, patterns were heated to 975 °C and prealloyed charges of Vit106 were lowered onto the patterns under high vacuum. After 3 min, during which time the alloy melted and formed a gas-tight seal against the crucible wall, high-purity argon was admitted to the crucible, forcing the molten alloy into the salt pattern. A 150 kPa pressure was maintained for 30–60 s to promote full infiltration, after which the crucibles were quenched in a strongly-agitated chilled 8.5 wt.% NaCl brine solution. Infiltrated samples were machined into uniform cylinders using a diamond grinding wheel and a diamond wafering saw.

Leaching of salt patterns was performed in 2 M nitric acid solutions, agitated either by magnetic stirring or ultrasound. After leaching, foam samples were left in acid baths until the target relative densities of 20–25% were achieved and then tested for crystallinity using CuK_α X-ray diffraction (XRD). All samples discussed herein were free of crystallinity within the limits of XRD detection. Scanning electron microscopy (SEM) was performed on a Hitachi S3500-N using secondary-electron imaging, and differential scanning calorimetry (DSC) measurements were performed in argon on an ISI DSC550 using a constant heating rate of 20 °C/min. Corrosion of Vit106 was tested in 200 ml HNO_3 and HCl baths of various concentrations at ambient temperature with different agitations. Quadrilateral test coupons were cut from plates of amorphous Vit106, polished with 1200 grit SiC paper, and thoroughly cleaned before immersion. Mass losses were measured after 24–48 h immersion, and estimated corrosion depths calculated from the measured surface areas under the assumption of uniform corrosion.

3. Results and discussion

3.1. Pattern selection

In the production of aluminum foams by the replication method, NaCl is the pattern material of choice due to its high melting point (relative to aluminum) and high solubility in water [10,13]. The melting point of NaCl is not, however, sufficiently high to allow its use as a pattern for Vit106, which requires processing temperatures about 130 °C [14] above its liquidus (842 °C) [8,15] in order to preserve its full glass-forming ability. Such temperatures, given the stringent purity requirements of glass-forming metallic melts and the high contact area between infiltrated melt and salt pattern, preclude the use of bromide, iodide, and chloride salts, as well as many fluoride salts. There are several fluorides, nonetheless, with melting points well in excess of 975 °C, including the highly-stable alkaline earth fluorides MF_2 (M = Mg, Ca, Sr, or Ba) [16]. Among these, SrF_2 and BaF_2 were selected for study based on their high melting points of 1477 °C and 1368 °C, respectively [16].

3.2. Pattern creation

Among the various sintering atmospheres tested (high vacuum, low vacuum and argon), high vacuum conditions gave for both salts the best overall balance among pattern mechanical integrity, contamination/reaction with graphite, and evaporation losses. Accessible sintering temperatures for BaF_2 in high-vacuum conditions were limited to 1250–1275 °C (homologous temperature 0.93–0.94) by evaporation losses; the equilibrium vapor pressures of BaF_2 in this temperature range are 5–12 Pa [17], well above the working pressure maintained by the vacuum furnace. Conversely, SrF_2 was effectively sintered under the same conditions at temperatures as high as 1400–1440 °C (homologous temperature 0.96–0.98), in which range it has comparable vapor pressure (5–10 Pa) [18]. It is noteworthy that early attempts to use water-soluble NaF (melting point: 996 °C) [16] as a pattern material for Vit106 led to attack of Vit106 charges by salt vapor during melting, preventing pooling of the alloy as required for melt infiltration. Equilibrium vapor pressures for SrF_2 and BaF_2 at the infiltration temperature of 975 °C are 2×10^{-4} Pa and 6×10^{-3} Pa, respectively, [18] posing little threat to the alloy.

No densification was observed for either salt under any sintering conditions, even with BaF_2 powders as fine as 100–150 μm. Lack of densification during sintering is well established for NaCl, a result of the fact that the dominant mechanism of sintering in NaCl is evaporation–condensation, as opposed to bulk or grain boundary diffusion [19]. Densification in NaCl is observed only when particle size is sufficiently small, around

100–150 μm [19]. It is expected that the critical particle sizes for SrF_2 and BaF_2 lie below that of NaCl; however, powders finer than 100 μm were not investigated in the present work, in order to minimize infiltration times and pressures, contact area with the molten alloy and leaching times. For this reason, the final packing density of sintered SrF_2 and BaF_2 patterns reported here was equal to the tap-dense packing fraction, 50 ± 2% (errors represent one standard deviation). This may also be taken as the initial volume fraction of Vit106 in infiltrated samples, i.e. the initial 'relative density' of all foams.

3.3. Pattern removal

Although both BaF_2 and SrF_2 have measurable solubilities in water [16], early experiments confirmed that leaching patterns in water alone, particularly from infiltrated samples, was not feasible. By contrast, both salts were susceptible to dissolution in strong acids. Although the exact mechanism for this dissolution is unclear, it has been suggested that BaF_2 dissolves in HNO_3 through the formation of $Ba(NO_3)_2$ and HF [20]. Similar exchange reactions likely describe the dissolution of BaF_2 in HCl and SrF_2 in HCl and HNO_3. The capacity of these acids to dissolve SrF_2 and BaF_2 may then be attributed to the high aqueous solubilities of acidified HF, $(Sr,Ba)(NO_3)_2$, and $(Sr,Ba)Cl_2$ [16].

In an effort to identify the ideal leaching conditions for pattern removal from infiltrated Vit106 foams, mass loss measurements on monolithic coupons (mass: 0.75–1.0 g) of amorphous Vit106 were made for a range of different bath conditions in both HCl and HNO_3 solutions. Evidence of localized corrosion (pitting) on these coupons was seen after 24 h immersion in stagnant 2–4 M HCl, while at concentrations of 8 M and above, massive macroscopic damage was observed. Attempts to leach infiltrated samples using even lower (<2 M) HCl concentrations led to low dissolution rates with visible discoloration of the alloy, such that HCl was not further investigated.

Fig. 1 shows coupon mass loss results using various HNO_3 baths. For acid concentrations between 1 M and 8 M, no mass losses were measured after 24-h immersion in stagnant pure acid. Addition of 5–8 mM BaF_2 (simulating the fluoride concentration present during dissolution of infiltrated BaF_2 patterns) to HNO_3 baths led to measurable mass losses over the same series of concentrations, with comparable magnitude for all concentrations tested. Comparison of the data in Fig. 1 with literature data [20] for dissolution of BaF_2 in nitric acid shows that the maximum ratio of salt dissolution rate to alloy corrosion rate is achieved with 2 M HNO_3, which was selected on this basis as the optimal bath concentration for salt removal with minimal alloy loss. Agitation (using a magnetic stir bar) of fluoride-bearing HNO_3 solutions led to four- to fivefold increases

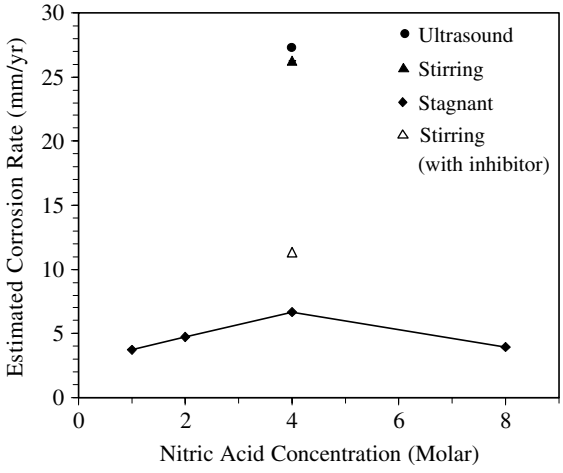

Fig. 1. Rate of attack of amorphous Vit106 coupons in nitric acid baths at ambient temperature containing dissolved BaF_2 in proportions chosen to simulate full dissolution of patterns from infiltrated samples (typical concentration: 5–8 mM). The hollow triangle demonstrates the potential benefits of corrosion inhibitors (in this case, fine alumina powder), which reduce the aggressiveness of fluoride ion liberated by the dissolving salt.

in coupon mass loss (Fig. 1), presumably due to the higher concentration and mobility of dissolved atmospheric oxygen in the stirred baths. Ultrasonic agitation did not significantly alter corrosion rates relative to magnetic stirring; however, infiltrated Vit106/BaF_2 samples showed initial rates of mass loss (measured after 4 h immersion) eight times higher for ultrasonic agitation compared to stirring in 2 M HNO_3, after normalizing for sample surface area. This may have resulted from breakup or debonding of the BaF_2 particles in ultrasonic baths, increased acid convection within the foam cells, or enhanced removal of $Ba(NO_3)_2$ or other dissolution intermediates formed on the surface of BaF_2 exposed to nitric acid, with attendant increases in overall salt dissolution rate. In any case, ultrasonic agitation undoubtedly lowers the immersion time required for pattern removal, and thereby lowers the overall loss of alloy during leaching.

Corresponding measurements using HNO_3 containing dissolved SrF_2 were not made, after early observations showed that dissolution rates for Vit106/SrF_2 samples, in acid concentration ranges where Vit106 coupons corroded uniformly, were impractically low.

3.4. Vit106 foams

Fig. 2a–c shows representative SEM images from a Vit106 foam of nominal pore size 212–250 μm (final pore size is higher than initial salt particle size due to alloy dissolution) and relative density 22% following removal of its BaF_2 pattern by 16 h immersion in ultrasonically-agitated 2 M nitric acid. Pattern removal was likely completed after only 4 h immersion, based on an inflection in

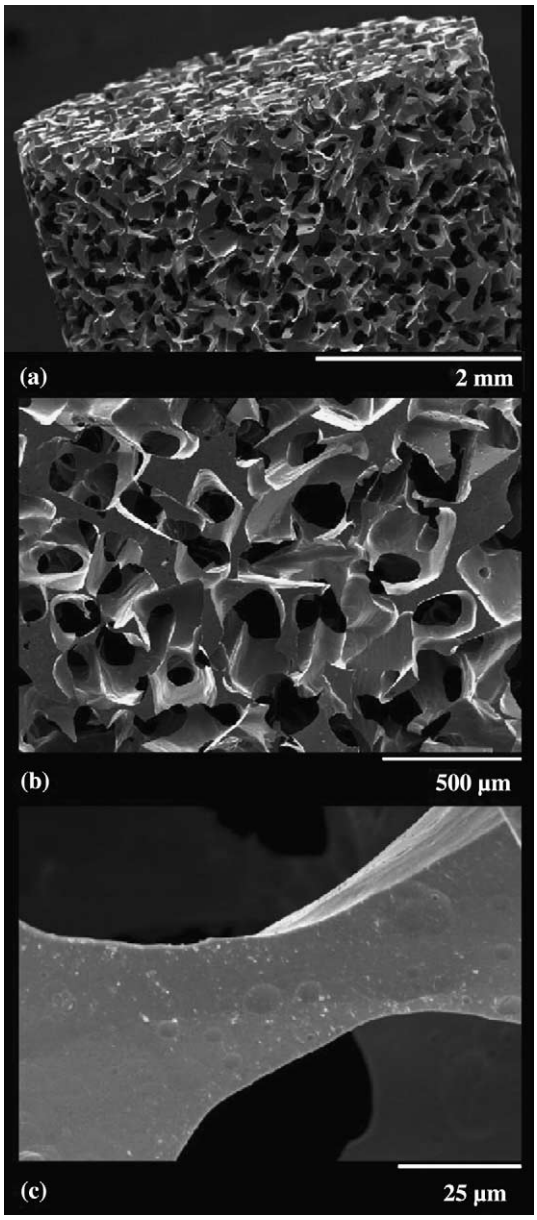

Fig. 2. SEM micrographs of an amorphous Vit106 foam (diameter: 4.5 mm, relative density: 22%) after pattern removal in ultrasonically-agitated 2 M nitric acid. (a) Uniform macrostructure of the foam. (b) Surface of the foam, showing sockets left behind by individual BaF_2 particles. (c) Individual foam strut, having high aspect ratio. The surface of this strut shows small indentations ('scalloping') produced by the corrosive leaching bath.

a plot of mass loss vs. time, which occurred at a mass loss equal to that predicted based on initial sample mass and volume fractions. The foam was then replaced into a fresh bath for an additional 12 h in order to continue lowering its relative density by alloy dissolution to a target value of 20–25% (using this process, a similar foam was reduced to about 15% density), chosen to demonstrate that foam density can be tailored through dissolution without incurring excessive damage to the foam. The structure of this foam is highly uniform and has a high proportion of mass localized at the nodes where struts meet. Such localization has been observed previously in aluminum foams made by the salt replication method [21], and is a result of the geometry of the salt particles and the resulting interstices within the sintered salt patterns. It is expected to be mechanically inefficient, as it leads to higher foam density for a given strut thickness (and hence load-bearing capacity). Such mechanical inefficiency is often acceptable given the exceptional uniformity and fine control over pore size and morphology achievable in replicated foams.

Fig. 2c shows an individual strut within the foam. This strut, like all features in the foams reported here, is well below the limiting thickness of about 1 mm required for Vit106 ductility [9]. The strut shown also has a sufficiently high aspect ratio to favor the necessary bending deformation, in contrast to the more equiaxed nodal regions, which are expected to fail with minimal plasticity. The strut surface in Fig. 2c exhibits a 'scalloped' texture (characterized by the presence of shallow circular pits or craters) that is common to all the Vit106 surfaces within the foams following acid leaching. This texture is not seen on foam surfaces prior to leaching, and is therefore believed to result from corrosive attack of the alloy by the fluoride-bearing acid bath during pattern removal, perhaps localized attack occurring at small crystalline surface inclusions. Protection of Vit106 against such attack might be accomplished through impressed current polarization, sacrificial anodes, or the use of inhibitors. Though no information is currently available regarding the corrosion chemistry of Vit106 in the aggressive media used here, the high zirconium content of Vit106 may prove useful by allowing methods for corrosion mitigation in Zr alloys to be applied to Vit106. For example Zr alloys are known to be passive in HNO_3 but highly susceptible to passive film disruption by fluoride [22,23], in qualitative agreement with observations presented here. Accordingly, inhibiting additives such as alumina, silica, $Al(NO_3)_3$, and P_2O_5 have been developed to lower the aggressiveness of fluoride towards Zr, e.g. by binding it into inert complexes [22,23]. A preliminary example of this effect is shown in Fig. 1, where the rate of corrosion of a Vit106 coupon in stirred fluoride-bearing 4 M nitric acid containing 75 g/l fine (6–23 μm) Al_2O_3 powder is shown. Compared to the same solution without Al_2O_3, the corrosion rate has been more than halved.

Nevertheless, alloy corrosion during uninhibited leaching of Vit106/BaF_2 samples was significant even for the most rapid dissolution conditions (ultrasonic 2 M HNO_3), as demonstrated by the fact that the foam of Fig. 2 dissolved at an appreciable rate in the ultrasonic bath even after the removal of nearly all of its BaF_2 pattern. Further evidence of corrosion was present in DSC data obtained from foam samples. As shown in Fig. 3, foam samples exhibited an additional exothermic feature

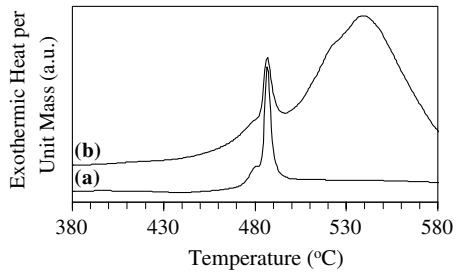

Fig. 3. DSC data from (a) monolithic amorphous Vit106 and (b) amorphous Vit106 foam following pattern removal in stagnant nitric acid. The exothermic peaks beginning around 474 °C in each curve represent crystallization of Vit106, while the broad exothermic peak centered at 540 °C in the foam is due to buildup of corrosive fluoride in stagnant regions of acid inside the foam. This peak is still present, with much reduced magnitude, in foams leached using stirred or ultrasonic baths (not shown).

superimposed onto the bulk signal arising from the glass and crystallization transitions of the Vit106 (onsets at 399 and 474 °C, respectively). In fully leached foam samples, this exotherm was quite pronounced; in monolithic samples of Vit106 exposed to a simulated leaching bath of fluoride-bearing 2 M nitric acid, the feature persisted with smaller magnitude. In monolithic Vit106 exposed to pure 2 M nitric acid, the feature had even smaller magnitude. These observations suggest that the signal arose from a corrosion product of Vit106, accelerated by exposure to fluoride, rather than from contamination or microstructural changes incurred during the casting process. This view is further supported by the fact that the total heat release associated with the exotherm did not scale with sample mass or volume, and hence most likely reflected a surface reaction (though without an accurate measure of the surface areas of small foam DSC samples, this cannot be quantified). Although the exotherm obscured the small endothermic glass transition in foam samples, it is notable that the onset of crystallization in the foam was essentially unchanged from the unprocessed monolithic alloy, suggesting that contact between the molten alloy and the salt pattern only minimally affected the BMG. This view is supported by the fact that infiltrated Vit106/BaF_2 samples of 7 mm diameter were fully vitrified, compared to a maximum castable diameter of about 10 mm for monolithic Vit106 [24].

4. Conclusions

Amorphous metal foams show great potential as alternatives to monolithic BMG alloys, having lower density and far superior ductility, and as alternatives to crystalline metallic foams, having improved strength and corrosion resistance with manageable processing temperatures. In this report, we have demonstrated for the first time successful processing of open-cell foams from a commercial Zr-based BMG alloy using the salt replication technique, and outlined and discussed several key factors in their production. Open-cell Zr-based BMG foams may eventually find application as lightweight structural materials, corrosion-resistant filters or catalyst substrates, or bone replacement materials.

Acknowledgment

The authors acknowledge the support of the Defense Advanced Research Project Agency's Structural Amorphous Metals (DARPA-SAM) program and the Caltech Center for Structural Amorphous Metals.

References

[1] Ashby MF, Evans AG, Fleck NA, Gibson LJ, Hutchinson JW, Wadley HNG. Metal Foams: A Design Guide. Boston: Butterworth-Heinemann; 2000.
[2] Banhart J. Prog Mater Sci 2001;46:559.
[3] Inoue A. Acta Mater 2000;48:279.
[4] Wang WH, Dong C, Shek CH. Mater Sci Eng 2004;R44:45.
[5] Apfel RE, Qiu N. J Mater Res 1996;11:2916.
[6] Schroers J, Veazey C, Johnson WL. Appl Phys Lett 2003;82:370.
[7] Wada T, Inoue A. Mater Trans 2003;44:2228.
[8] Brothers AH, Dunand DC. Appl Phys Lett 2004;84:1108.
[9] Conner RD, Johnson WL, Paton NE, Nix WD. J Appl Phys 2003;94:904.
[10] Polonsky L, Lipson S, Markus H. Modern Castings 1961;39:57.
[11] Pekala RW, Hopper RW. J Mater Sci 1987;22:1840.
[12] Fitzgerald TJ, Michaud VJ, Mortensen A. J Mater Sci 1995;30:1037.
[13] San Marchi C, Mortensen A. In: Degischer HP, Kriszt B, editors. Handbook of Cellular Metals: Production, Processing, Applications. Weinheim: Wiley-VCH; 2002. Chapter 2.
[14] Lin XH, Johnson WL, Rhim WK. Mater Trans JIM 1997;38:473.
[15] Choi-Yim H, Busch R, Koster U, Johnson WL. Acta Mater 1999;47:2455.
[16] Lide DR, editor. Handbook of Chemistry and Physics. 81st Ed., New York: CRC Press; 2000.
[17] Hart PE, Searcy AW. J Phys Chem-US 1966;70:2763.
[18] Bautista RG, Margrave JL. J Phys Chem-US 1965;69:1770.
[19] Thompson RJ, Munir ZA. J Am Ceram Soc 1982;65:312.
[20] Smirnov AE, Urusovskaya AA. J Mater Sci 1980;15:1183.
[21] San Marchi C, Mortensen A. Acta Mater 2001;49:3959.
[22] Schweitzer PA. Corrosion Engineering Handbook. New York: Marcel Dekker; 1996.
[23] Petit JA, Chatainier G, Dabosi F. Corros Sci 1981;21:279.
[24] Choi-Yim H, Conner RD, Szuecs F, Johnson WL. Acta Mater 2002;50:2737.